Fracture behaviour of carbon fibre/epoxy composites interleaved by MWCNT- and graphene nanoplatelet-doped thermoplastic veils

Quan, Dong; Mischo, Chiara; Binsfeld, Lucas; Ivankovic, Alojz; Murphy, Neal

DOI
10.1016/j.compstruct.2019.111767

Publication date
2020

Document Version
Accepted author manuscript

Published in
Composite Structures

Fracture behaviour of carbon fibre/epoxy composites interleaved by MWCNT- and graphene nanoplatelet-doped thermoplastic veils

Dong Quan[a], Chiara Mischo[b], Lucas Binsfeld[b], Alojz Ivankovic[b], Neal Murphy[b,*]

[a]*Structural Integrity & Composites Group, Faculty of Aerospace Engineering, Delft University of Technology, Netherlands*

[b]*School of Mechanical and Materials Engineering,University College Dublin, Ireland*

Abstract

Polyphenylene-sulfide (PPS) veils doped with MWCNTs and graphene nanoplatelets (GNPs) were used as interleaves of a carbon fibre/epoxy composite, aiming to study its effects on the fracture performance. Interlaying original PPS veils significantly improved the mode-I and mode-II fracture toughness of the laminates due to a PPS fibre bridging mechanism. The addition of MWCNTs on the veils improved the PPS fibre/epoxy adhesion by introducing additional interactions, i.e. MWCNT pull-out and breakage, between the PPS fibres and the epoxy during the fracture process. This further improved the fracture toughness of the laminates at a relatively low content of MWCNTs. In contrast, the incorporation of GNPs on the veils decreased the PPS fibre/epoxy adhesion, resulting in detrimental effects on the fracture performance.

Keywords: Polymer matrix composites, Fracture toughness, Thermoplastic veils, MWCNTs, Graphene.

*Corresponding author. Tel: +353 (1) 7161940; Email: neal.murphy@ucd.ie (Neal Murphy)

1. Introduction

The poor interlaminar fracture toughness of carbon fibre reinforced plastics (CFRPs) is a major constraint on their wider use for structural applications. For this reason, toughening CFRPs has been a focus of research over the last few decades, with many methods proposed, such as blending second phase modifiers with the epoxy matrix [1, 2]; 3D weaving [3], stitching [4, 5] and Z-pinning [6, 7] of the carbon fibre fabrics; and interlaying different materials between the adjacent carbon fibre fabrics [8–10]. Among them, interlayer toughening is a simple and promising process that does not necessarily add significant cost to the fabrication of a composite. Various types of materials were used as interleaves to reinforce fibre reinforced plastics (FRPs), with thermoplastic veils [11], thermoplastic films [12], short fibres [8], carbon nanotubes/fibres [13] and graphene [14] representing the most prevalent candidates.

The excellent mechanical properties of carbon nanotubes (CNTs) and graphene make them attractive options as toughening agents of FRPs. In general, CNTs and graphene were introduced to the CFRPs by three means: (1) blending them into the epoxy matrix [2, 15]; (2) grafting them directly onto the carbon fibre fabrics [16–18]; and (3) incorporating them as interleaves between the adjacent carbon fibre plies [19, 20]. To be used as interleaves, CNTs and graphene were normally hybridised with a second phase material, such as short carbon fibres [8, 19], epoxy resin [14, 21] and thermoplastic film [22]. Encouraging improvements in the fracture toughness have been achieved by using different hybrid interleaves. For instance, Zhou et al. [8] employed CNT-decorated short carbon fibres (CNT-SCF) as interleaves of CFRPs, and observed a 125 % increase in the mode-I fracture toughness. In other studies [14, 21], graphene was mixed with epoxies and then used as interleaves of CFRPs, showing an increase of above 100 % in the mode-I fracture toughness. Apart from tailoring the mechanical properties of polymer composites, CNTs and graphene have also shown considerable promise to improve the electrical conductivity [23–25].

Thermoplastic veils are tough, ductile polymer networks possessing porous structure and light weight. These unique features distinguish them from the other candidates as interleaves of FRPs, i.e. their porous structure will not hinder resin impregnation during the composite manufacture, the high specific surface area of the thin thermoplastic fibres can promote bonding to the matrix phase, and their thin and light nature means there is little compromise on composite weight and thickness [26]. Thermoplastic veils based on a wide variety of polymers, such as Polyamide (PA) [27, 28], Polyethersulfone (PES) [29], Polyphenylene sulfide (PPS) [30], Aramid [31], Polyether ether ketone (PEEK) [30], Polyvinyl alcohol (PVA) [32] and Polyacrylonitrile (PAN) [33], have been used as interleaves to toughen CFRPs. A review on the mechanical properties of FRPs interleaved by thermoplastic veils [9] suggested that interlaying thermoplastic veils within the FRPs can dramatically enhance their interlaminar fracture toughness. However, the significant improvements in the mechanical properties of CFRPs upon interlaying thermoplastic veils were offset by detrimental effects on the electrical conductivities [34, 35], which limited their used in aircraft structures[36]. This problem has been addressed in [25, 35] by incorporating MWCNTs in association with the thermoplastic veils, i.e. an increase of up to 227 % in the through-thickness electrical conductivity of the laminates was reported by Dydek et al. [25].

Based on the literature review, it is clear that interlaying hybrid interleaves consisting of thermoplastic veils and carbon nanomaterials has a significant potential to develop pioneer CFRPs with excellent mechanical and electrical properties. To date, the fracture behaviour of this type of composite system has received little attention. Therefore, the aim and main novelty of this project was to study the effects of MWCNT- and GNP-doped thermoplastic veils on the fracture performance of interleaved CFRPs. Different areal densities of MWCNTs and graphene nanoplatelets (GNPs) were doped on a PPS veil using a spray coating technique and then used to interlay an aerospace-grade CFRP. The mode-I and mode-II fracture behaviour

of the CFRPs were studied, and the corresponding fracture mechanisms were analysed.

2. Experimental

2.1. Materials

The carbon fibres were unidirectional carbon-fibre/epoxy prepreg (HYE 1034E) from Cytec (Solvay Group). The prepreg possessed an areal density of 230 g/m^2, and a fibre volume fraction of 57-63 %. The Polyphenylene sulfide (PPS) veils were supplied by Technical Fibre Products, UK. They possessed an areal density of 5 g/m^2, and will be referred to as PPS5 throughout this paper. The MWCNTs in an entangled cotton-like form were obtained from Graphene Supermarket, USA. They had an average outer diameter of 50-85 nm and a length of 10-15 μm. These MWCNTs were not functionalized and were used as-received. The graphene nanoplatelets (GNPs) were obtained in powder form from Graphene Supermarket, USA. These GNPs had an average flake thickness of 5-30 nm and an average particle lateral size of 5-25 μm.

2.2. Preparation of interleaved CFRPs

The MWCNTs and GNPs were doped on the PPS5 veils using an airbrush technique. The MWCNT or GNP powders were firstly well dispersed in acetone by a mechanical pre-mixing (IKA RW20 digital mixer) step at a speed of 500 rpm for 10 mins, followed by a high shear mixing (Silverson L4RT) process at a speed of 3000 rpm for 2 hours, and finally an ultrasonic mixing step at 26 kHz for 2 hours. The acetone was regularly topped-up during the mixing process to assure a concentration of 0.002 g/ml for the MWCNTs and 0.005 g/ml for the GNPs. The solution was then evenly sprayed on both sides of a layer of PPS veil using an airbrush with a nozzle size of 0.8 mm under an air pressure of 40 psi. The airbrush was positioned perpendicular to the PPS veils at a distance of 30 cm during the spraying process. The

veils were inverted mid-way through the spraying process, in order to get an even distribution of the MWCNTs or GNPs on both faces. The areal densities of the MWCNTs and GNPs were controlled by the amount of the solution sprayed onto the veils and were calculated based on the weight of the veils before and after spraying for an accurate measure. This spraying procedure was optimised after various trials to obtain an even distribution of the MWCNTs and GNPs. In this paper, the MWCNT- and GNP-doped veils will be referred to as the material type followed by its areal density. For example, PPS5CNT0.25 represents a PPS veil with an areal density of 5 g/m^2 containing 0.25 g/m^2 MWCNTs, and L/PPS5CNT0.25 represents the laminate interleaved by the PPS5CNT0.25 veils. Typical photographs of PPS veils doped without and with 1.1 g/m^2 MWCNTs and 1.0 g/m^2 GNPs are shown in Figure 1. It was found that the veils changed to a black colour by adding a small amount of MWCNTs and GNPs, and the distribution of the MWCNTs and GNPs appeared to be good at this scale. To further study the morphologies of the PPS fibres, MWCNTs and GNPs, samples with a size of approximately 10 mm$\times$10 mm were cut from the veils and gold sputtered for 20 s, and then imaged using a scanning electron microscope (Regulus8230 from Hitachi).

A layup consisting of 26 plies of the carbon fibre prepregs and one layer of veils at the mid-plane was prepared using a hand layup process. It should be noted that the veils were dried in an oven at 50 °C for 30 mins immediately before the layup process. To generate the crack starter for the fracture test samples, a PTFE insert (with a thickness of 12.5 μm) was also placed at the approperiate location of the mid-plane during the layup procedure. The layup was firstly consolidated under vacuum for 45 mins. It was then cured inside an in-house pressclave under vacuum and a pressure of 80 psi (approximately 5.5 bar) from the top. The cure cycle was a 2-hour linear ramp from room temperature to 180 °C followed by a 2-hour dwell at 180 °C. The laminate was allowed to cool down naturally to 80 °C under full pressure and vacuum to avoid post-curing warpage. The composite laminate was taken

out of the mould after the temperature dropped to room temperature, and was cut into the required dimensions for the fracture tests. Samples without veils, as a control, were also manufactured.

2.3. Test procedure

A double cantilever beam (DCB) test and an end loaded split (ELS) test were carried out to measure the mode-I and mode-II fracture energies according ISO15024 [37] and ISO15114 [38], respectively. A 5 mm long precrack from the crack starter was generated by loading the samples under an opening mode for both DCB and ELS specimens. A constant displacement rate of 2 mm/min and 1 mm/min was used for the DCB tests and the ELS tests, respectively. The crack initiation values for G_{IC} and G_{IIC} were determined using the 5% offset approach [37, 38]. At least three replicate tests were conducted for each case. Specimens with a size of approximately 10 mm$\times$10 mm were cut from the fractured DCB and ELS samples, and then gold sputtered and imaged by SEM to investigate the dominant fracture mechanisms.

3. Results and Discussion

3.1. Morphology of the MWCNT- and GNP- doped PPS fibres

Figure 2 shows typical SEM images of individual PPS fibres from the veils before and after doping with MWCNTs and GNPs. A neat and smooth surface was observed for the as-received PPS fibres, and the surfaces of the PPS fibres doped with carbon nanomaterials appeared much rougher due to the presence of numerous agglomerated MWCNTs and GNPs. Only a portion of the fibre surfaces was covered with MWCNTs and GNPs for the PPS fibres doped with 0.25 g/m^2 carbon nanomaterials, see the images for the CNT0.25 and GNP0.25 fibres in Figure 2. The entire surfaces of the PPS fibres were essentially covered in all the other cases, with a number of obvious lumps presenting on the CNT1.45 and GNP1.55 fibres.

3.2. Mode-I fracture

3.2.1. Mode-I fracture toughness

R-curves from the DCB laminate tests are shown in Figure 3, and the corresponding mode-I fracture initiation energy (G_{IC}^{ini}), and mode-I fracture propagation energy (G_{IC}^{prop}, taken as the average value of the plateau region of the R-curves) are summarised in Table 1. It was found that the L/Origin (CFRPs without thermoplastic veils) laminate possessed essentially 'flat' R-curves, indicating limited carbon fibre bridging during the fracture process (see Figure 3). Interlaying PPS5 veils to the L/Origin laminate resulted in considerable increases in the mode-I fracture toughness. i.e. G_{IC}^{ini} increased from 181 J/m^2 to 210 J/m^2, and G_{IC}^{prop} increased from 171 J/m^2 to 264 J/m^2, see Table 1. This was associated with a significantly 'rising' trend of the R-curves (before a crack length of 70 mm, see Figure 3), suggesting extensive fibre bridging during the fracture process. Doping a small amount of MWCNTs on the PPS veils further improved the mode-I fracture performance of the L/PPS5 laminate, e.g. G_{IC}^{ini} and G_{IC}^{prop} increased to above 240 J/m^2 and 290 J/m^2, respectively, for both the L/PPS5CNT0.25 and the L/PPS5CNT0.6 laminates. However, the mode-I fracture toughness strikingly dropped as the areal density of the MWCNTs increased to above 1.0 g/m^2. For example, G_{IC}^{prop} dramatically decreased from 299 J/m^2 to 181 J/m^2 as the areal density of the MWCNTs increased from 0.6 g/m^2 to 1.1 g/m^2, and further to 147 J/m^2 as the areal density of the MWCNTs increased to 1.45 g/m^2. This was accompanied with a plunge of the 'rising' trend of the R-curves for the L/PPS5CNT1.1 and L/PPS5CNT1.45 laminates in Figure 3 (a), demonstrating a considerable drop in the amount of fibre bridging during the fracture process. Unlike the MWCNTs, the significance of the 'rising' trend of the R-curves remained more or less the same level upon doping different amount of GNPs on the PPS5 veils, as shown in Figure 3 (b). The incorporation of GNPs on the PPS5 veils led to a steady drop in the mode-I fracture toughness of the laminates, see Table 1. G_{IC}^{prop} decreased from 264 J/m^2 to 249 J/m^2

upon doping 0.25 g/m^2 GNPs on the PPS5 veils, and further to 228 J/m^2 by adding 0.5 g/m^2 GNPs on the PPS5 veils, and then remained more or less the same as the areal density of the GNPs increased to 1.65 g/m^2.

3.2.2. Mode-I fracture mechanisms and discussion

Representative SEM images of the fracture surfaces of the DCB specimens are shown in Figure 4. It should be noted that a cohesive failure inside the thermoplastic veils took place for all the interleaved CFRPs in the current work. A large number of PPS fibres were observed on the fracture surface of the L/PPS5 laminate, with the majority of them being in a long and continuous form and the remainder being short with a free end (see Figure 4 (a)). The continuous and long PPS fibres were formed by extensive fibre bridging and pull-out of the fibres from the matrix during the fracture process, and the short PPS fibres (with a free end) were generated by either the breakage or the pull-out of one edge of the PPS fibres. These were the main toughening mechanisms of the PPS fibres, resulting in the considerable improvements of the fracture energy and the significantly 'rising' trend of the R-curves (as observed in Figure 3 and Table 1). Comparing the fracture surfaces of the L/PPS5 laminate (Figure 4 (a)) and those doped with MWCNTs (Figure 4 (b) and (c)), it was found that the quantity of long and continuous PPS fibres decreased due to the presence of the MWCNTs on the PPS fibres, and essentially disappeared as the areal density of the MWCNTs increased to above 1.0 g/m^2 (linked to the removal of the 'rising' trend of the R-curves for the L/PPS5CNT1.1 and L/PPS5CNT1.45 laminates in Figure 3 (a)). At the same time, more short PPS fibres with one end free and another end well-embedded in the matrix were observed as the areal density of the MWCNTs increased, indicating additional PPS fibre breakage. This clearly indicates an improved adhesion between the PPS fibres and the epoxy matrix due to the presence of MWCNTs. Figures 4 (e) and (f) show typical SEM images of the fracture surfaces of the L/PPSCNT1.1 laminate, with higher magnifications. Numerous MWCNT segments

were observed in the region along the PPS fibres, and they were formed by either pull-out or breakage of the MWCNTs [23, 39]. These interactions between the MWCNTs on the PPS fibres and the epoxy matrix contributed to the improvement of the PPS fibre/epoxy adhesion, and have been proven to be able to moderately increase the mode-I fracture energy of the epoxy matrix [2, 23, 39] and the CFRPs [2]. Hence, doping MWCNTs on the PPS5 veils introduced additional MWCNT pull-out and breakage at nano-scale, and subsequently improved the PPS fibre/adhesion and resulted in additional PPS fibre breakage at micro-scale. These mechanisms together with the PPS fibre bridging led to the best fracture performance of the L/PPS5MWCNT0.25 and L/PPS5MWCNT0.6 laminates. However, as the areal density of the MWCNTs increased to above 1 g/m^2, the PPS fibre bridging (the main toughening mechanism of the PPS5 veils) almost vanished since the PPS fibre/epoxy adhesion reached a level that is sufficient to prevent the delaminatation of the PPS fibres. This considerably decreased the length of the fracture process zone ahead of the crack tip and led to the dramatic drop in the fracture energy of the L/PPS5MWCNT1.1 and L/PPS5MWCNT1.45 laminates (see Table 1). Typical SEM images of the fracture surfaces of the L/PPS5GNP0.25 and L/PPS5GNP1.0 laminates are shown in Figures 4 (d) and (g). The fracture mechanisms of the laminates interleaved with GNP-doped PPS veils were observed to be the same as the L/PPS5 laminate at this scale, i.e. PPS fibre bridging and pull-out (evidenced by the long and continuous PPS fibres) and PPS fibre breakage (indicated by the short and broken PPS fibres). Figure 4 (h) and (i) show typical SEM images of the mode-I fracture surface of the L/PPS5GNP1.0 laminate at higher magnifications. The surface of the region containing GNPs (around the PPS fibres) was very rough owing to the crack deflections, which was identified to be the main toughening mechanism of the GNPs [40–42]. However, in the current work, all the GNPs attached on the surfaces of the PPS fibres, resulting in significant local agglomerations, as shown in Figure 2. In this case, crack propagation mainly took place be-

tween the GNP layers, which caused detrimental effects on the toughening performance of the GNPs [40–42]. Moreover, the coverage of the PPS fibres by the agglomerated 2D-structure GNPs decreased the adhesion between the PPS fibres and the epoxy matrix, and subsequently affected the toughening efficiency of the PPS veils through a fibre bridging mechanism. This explained why the addition of GNPs on the PPS5 veils decreased the mode-I fracture energy of the CFRPs.

3.3. Mode-II fracture

3.3.1. Mode-II fracture toughness

Figure 5 shows the R-curves from the laminate ELS tests. A stable crack propagation behaviour through the entire ELS testing region (between a crack length of 70-100 mm) was observed for the L/Origin laminate, evidenced by the 'flat' R-curves in Figure 5. However, the incorporation of interlayers resulted in a dynamic failure of the specimens for all the interleaved laminates, i.e. the crack dynamically failed the entire ELS specimens after a stable propagation of a few millimetres. Hence, there are only a few points on the R-curves of the interleaved laminates in Figure 5. Additionally, significantly 'rising' R-curves were observed for all the interleaved laminates, indicating an extension of the mode-II fracture process zone ahead of the crack tip due to the presence of fibre bridging. The mode-II fracture initiation energy (G_{IIC}^{ini}) and the mode-II fracture propagation energy (G_{IIC}^{avg}, taken as the average value of all the points on the R-curves) are summarised in Table 1. A value of 630 J/m^2 for G_{IIC}^{ini} and 627 J/m^2 for G_{IIC}^{avg} was measured for the L/Origin laminate. The incorporation of the original PPS5 veils as interlayers dramatically increased G_{IIC}^{ini} and G_{IIC}^{avg} to 1730 J/m^2 and 1868 J/m^2, respectively. Further improvements in the mode-II fracture energy were observed by adding 0.25 g/m^2 MWCNTs on the PPS5 veils, i.e. G_{IIC}^{ini} and G_{IIC}^{avg} further increased to 1892 J/m^2 and 1949 J/m^2, respectively. However, both G_{IIC}^{ini} and G_{IIC}^{avg} dropped to a value of around 1200 J/m^2 as the areal density of the MWCNTs increased to above 1 g/m^2. Similar

to the mode-I fracture, doping GNPs on the PPS5 veils resulted in a decrease in the mode-II fracture energy of the laminates, i.e. G_{IIC}^{ini} and G_{IIC}^{avg} steadily decreased to 1056 J/m^2 and 1151 J/m^2 respectively as the areal density of the GNPs increased to 1.65 g/m^2.

3.3.2. Mode-II fracture mechanisms and discussion

During the ELS tests of all the interleaved laminates, a mixture of cohesive failure (inside the veils) and interfacial failure (between the veils and the carbon fibre plies) took place, leaving the majority of the epoxy resin and the PPS fibres on the upper fracture surfaces, see Figure 6 as an example. Figure 7 presents representative SEM images of the fracture surfaces of the ELS specimens. In Figures 7 (a)-(d) and (g), the images on the left side of the red lines are for the resin-rich side of the fracture surfaces and the images on the right side of the red lines are for the resin-sparse side of the fracture surfaces. By comparing Figures 7 (b) and (c) to Figure 7 (a), it was found that the fracture surfaces of the L/PPS5 and L/PPS5CNT0.25 laminates appeared more or less the same, i.e. both sides of the fracture surfaces had a large number of long and continuous PPS fibres as a result of PPS fibre bridging during the fracture process. However, for the L/PPS5CNT1.1 laminate, all the PPS fibres were well embedded in the epoxy layer on the resin-rich side of the fracture surfaces, and the amount of PPS fibres and epoxy on the resin-sparse side significantly dropped, see Figure 7 (c). These observations further confirmed an improved PPS fibre/epoxy adhesion due to the presence of MWCNTs. Similarly to the mode-I fracture, a reasonably improved PPS fibre/epoxy adhesion can be beneficial for the mode-II toughness enhancement, since it can increase the required force to pull-out the PPS fibres and subsequently enhance the toughening efficiency of the fibre bridging mechanism. This, together with the MWCNT pull-out and breakage (evidenced by the presence of the MWCNT segments on the fracture surfaces [2, 43], see Figures 7 (e) and (f)) led to a further improvement of the fracture energy for doping 0.25 g/m^2 on the PPS5 veils, as shown in Table 1. However, as the PPS fibre/epoxy adhesion improved to a higher

level due to doping more MWCNTs on the veils, it deflected the crack from the inside of the veils (cohesive) to the boundary between the veils and the carbon fibres (interfacial). In this case, the main toughening mechanism of the PPS5 veils, i.e fibre bridging, was restrained. This caused the considerable drop in the mode-II fracture energy of the laminates as the areal density of the MWCNTs increased above 0.25 g/m^2, see Table 1. In contrast, doping GNPs on the PPS fibres reduced the PPS fibre/epoxy adhesion, as discussed in Section 3.2.2. For this reason, the PPS veils became a weaker path for the crack propagation, resulting in more PPS fibres and epoxy resin on the fracture surfaces of the resin-sparse side in Figures 7 (d) and (g) than in Figure 7 (a). A weaker PPS fibre/epoxy adhesion caused detrimental effects on the toughening efficiency of the PPS fibre bridging mechanism, and subsequently decreased the fracture toughness of the laminates. Figures 7 (h) and (i) present SEM images of the L/PPS5GNP1.0 laminates with higher magnifications, showing numerous GNPs flakes and deflected crack lines around the PPS fibres. These mechanisms were beneficial for the toughness enhancement of the laminates. However, since the GNPs largely agglomerated around the PPS fibres, the toughening performance of the GNPs was expected to be poor [40–42]. These combined influences as a result of doping GNPs on the PPS veils eventually resulted in a decrease in the mode-II fracture energy of the laminates, as observed in Table 1.

3.4. Discussion on the toughening performance of thermoplastic veils

Table 2 summarises the toughening performance of different thermoplastic veils for unidirectional carbon fibre/epoxy composites. The values in bold highlight the cases showing deteriorations in the fracture toughness. It is clear that adding both micro- and nano-scale veils can dramatically improve the interlaminar fracture toughness of CFRPs, i.e. the reviewed maximum improvements in G_{IC} and G_{IIC} were 281 % [44] and 211 % [45], respectively for adding nano-fibre veils, and 718 % [27] and 211 % (the current work), respectively for interlaying micro-fibre veils. However, significantly varied values for the toughening levels were

reported in different studies, with some of them exhibiting detrimental effects on the fracture toughness (highlighted in bold). The findings of this work showed that the adhesion between the thermoplastic veils and the epoxy matrix significantly affected the fracture mechanisms, and hence the fracture energies of the interleaved laminates. Apart from this, the toughening levels of interlaying thermoplastic veils can be linked to many other factors, including the areal density of the veils [26–28, 45], the veil material [26, 46–48], the form of the veils in the FRPs, i.e. melted or non-melted [48–50] and the architecture of the carbon fibre fabrics [45–47, 51]. Unfortunately, to date, no definitive conclusions regarding any of these factors can be drawn based on the literature, owing to the inherent complexities and the lack of systematic studies. For instance, it is unreasonable to make a conclusion by comparing the results from different studies, as the toughening interlayers, CFRP systems and manufacturing processes differed significantly between different cases. Accordingly, systematic studies considering all the key affecting parameters are still required to further understand the technique of interlaying thermoplastic veils for CFRP toughening. Overall, a comparison between the results of the current work and the other literature in Table 2 indicates that the toughening levels of MWCNT- and GNP- doped thermoplastic veils are competitive. This, together with the findings of our previous work [35] demonstrated an obvious feasibility of using MWCNT-/GNP-doped thermoplastic veils to simultaneously improve the interlaminar fracture toughness and electrical conductivities of CFRPs. Such materials are desirable for applications that require good resistance to lightening strikes, such as the exterior of aircraft and wind turbine blades. They can also be used for electromagnetic shielding and damage detection applications.

4. Conclusions

This work studied the mode-I and mode-II fracture energies and mechanisms of an aerospace-grade CFRP interleaved with MWCNT- and graphene nanoplatelet (GNP)-doped Polyphenylene-sulfide (PPS) veils. The main toughening mechanism of the PPS veils was PPS fibre bridging during the fracture process, which resulted in significant increases in the mode-I and mode-II fracture energy of the laminates. The addition of MWCNTs introduced additional interactions, i.e. MWCNT pull-out and breakage, between the PPS fibres and the epoxy matrix. This resulted in an improved PPS fibre/epoxy adhesion, and subsequently led to additional PPS fibre breakage and improved toughening performance of the fibre bridging mechanism during the fracture process. For these reasons, the fracture energy was further increased by doping a small amount of MWCNTs on the PPS veils. However, as more MWCNTs were doped on the veils, the PPS fibre/epoxy adhesion increased to a level that was sufficient to prevent the PPS fibre pull-out and bridging (the main toughening mechanism of the PPS veils). This caused a considerable drop in the fracture energy. In contrast, the 2D-structured GNPs significantly agglomerated and attached to the PPS fibres. This resulted in a drop of the PPS fibre/epoxy adhesion. In this case, a low force was required to pull-out the PPS fibres from the epoxy, resulting in detrimental effects on the toughening efficiency of the fibre bridging mechanism. Hence, doping GNPs on the PPS veils resulted in a steady drop in the fracture energy of the CFRPs.

Acknowledgements

The authors gratefully acknowledge the financial support from the Irish Composites Centre. We would also like to thank Bombardier Aerospace (UK) and Technical Fibre Products (UK) for supplying the carbon fibre fabrics and thermoplastic veils employed in this study.

Dong Quan received funding from the European Union's Horizon 2020 research and innovation programme under the Marie Skłodowska-Curie grant agreement No. 842467.

Data Availability

The raw/processed data required to reproduce these findings cannot be shared at this time due to legal or ethical reasons.

References

[1] S. Roy, A. Kumar, Effect of particle size on mixed-mode fracture of nanographene reinforced epoxy and mode I delamination of its carbon fiber composite, Composite Structures 181 (2017) 1 – 8, https://doi.org/10.1016/j.compstruct.2017.08.079.

[2] D. Quan, J. L. Urdaniz, A. Ivankovic, Enhancing mode-I and mode-II fracture toughness of epoxy and carbon fibre reinforced epoxy composites using multi-walled carbon nanotubes, Materials & Design 143 (2018) 81 – 92, https://doi.org/10.1016/j.matdes.2018.01.051.

[3] M. Pankow, B. Justusson, M. Riosbaas, A. M. Waas, C. F. Yen, Effect of fiber architecture on tensile fracture of 3D woven textile composites, Composite Structures 225 (2019) 111139, https://doi.org/10.1016/j.compstruct.2019.111139.

[4] J. Tapullima, C. H. Kim, J. H. Choi, Analysis and experiment on DCB specimen using I-fiber stitching process, Composite Structures 220 (2019) 521 – 528, https://doi.org/10.1016/j.compstruct.2019.04.020.

[5] K. P. Plain, L. Tong, The effect of stitch incline angle on mode I fracture toughness - Experimental and modelling, Composite Structures 92 (7) (2010) 1620 – 1630, https://doi.org/10.1016/j.compstruct.2009.11.027.

[6] J. Hoffmann, G. Scharr, Pull-out performance of rectangular z-pins in hot-cured carbon fiber reinforced laminates, Composite Structures 186 (2018) 62 – 67, https://doi.org/10.1016/j.compstruct.2017.11.080.

[7] L. W. Byrd, V. Birman, The estimate of the effect of z-pins on the strain release rate, fracture and fatigue in a composite co-cured z-pinned double cantilever beam, Composite Structures 68 (1) (2005) 53 – 63, https://doi.org/10.1016/j.compstruct.2004.02.014.

[8] H. Zhou, X. Du, H.-Y. Liu, H. Zhou, Y. Zhang, Y.-W. Mai, Delamination toughening of carbon fiber/epoxy laminates by hierarchical carbon nanotube-short carbon fiber interleaves, Composites Science and Technology 140 (2017) 46–53, https://doi.org/10.1016/j.compscitech.2016.12.018.

[9] R. Palazzetti, A. Zucchelli, Electrospun nanofibers as reinforcement for composite laminates materials-A review, Composite Structures 182 (2017) 711 – 727, https://doi.org/10.1016/j.compstruct.2017.09.021.

[10] D. Quan, S. Flynn, M. Artuso, N. Murphy, C. Rouge, A. Ivankovic, Interlaminar fracture toughness of CFRPs interleaved with stainless steel fibres, Composite Structures 210 (2019) 49 – 56, https://doi.org/10.1016/j.compstruct.2018.11.016.

[11] L. Daelemans, A. Cohades, T. Meireman, J. Beckx, S. Spronk, M. Kersemans, I. D. Baere, H. Rahier, V. Michaud, W. V. Paepegem, K. D. Clerck, Electrospun nanofibrous interleaves for improved low velocity impact resistance of glass fibre reinforced composite laminates, Materials & Design 141 (2018) 170 – 184, https://doi.org/10.1016/j.matdes.2017.12.045.

[12] C. H. Wang, K. Sidhu, T. Yang, J. Zhang, R. Shanks, Interlayer self-healing and toughening of carbon fibre/epoxy composites using copolymer films, Com-

posites Part A: Applied Science and Manufacturing 43 (3) (2012) 512 – 518, https://doi.org/10.1016/j.compositesa.2011.11.020.

[13] M. Arai, J. ichi Hirokawa, Y. Hanamura, H. Ito, M. Hojo, M. Quaresimin, Characteristic of mode I fatigue crack propagation of CFRP laminates toughened with CNF interlayer, Composites Part B: Engineering 65 (2014) 26 – 33, https://doi.org/10.1016/j.compositesb.2014.02.025.

[14] H. Ning, J. Li, N. Hu, C. Yan, Y. Liu, L. Wu, F. Liu, J. Zhang, Interlaminar mechanical properties of carbon fiber reinforced plastic laminates modified with graphene oxide interleaf, Carbon 91 (2015) 224 – 233, https://doi.org/10.1016/j.carbon.2015.04.054.

[15] M. Rahman, S. Zainuddin, M. Hosur, C. Robertson, A. Kumar, J. Trovillion, S. Jeelani, Effect of NH2-MWCNTs on crosslink density of epoxy matrix and ILSS properties of e-glass/epoxy composites, Composite Structures 95 (2013) 213 – 221, https://doi.org/10.1016/j.compstruct.2012.07.019.

[16] D. C. Davis, J. W. Wilkerson, J. Zhu, D. O. O. Ayewah, Improvements in mechanical properties of a carbon fiber epoxy composite using nanotube science and technology, Composite Structures 92 (11) (2010) 2653 – 2662, https://doi.org/10.1016/j.compstruct.2010.03.019.

[17] Z. Zhao, K. Teng, N. Li, X. Li, Z. Xu, L. Chen, J. Niu, H. Fu, L. Zhao, Y. Liu, Mechanical, thermal and interfacial performances of carbon fiber reinforced composites flavored by carbon nanotube in matrix/interface, Composite Structures 159 (2017) 761 – 772, https://doi.org/10.1016/j.compstruct.2016.10.022.

[18] X. Yao, X. Gao, J. Jiang, C. Xu, C. Deng, J. Wang, Comparison of carbon nanotubes and graphene oxide coated carbon fiber for improving the interfacial properties of car-

bon fiber/epoxy composites, Composites Part B: Engineering 132 (2018) 170 – 177, https://doi.org/10.1016/j.compositesb.2017.09.012.

[19] S.-H. Lee, H. Kim, S. Hang, S.-K. Cheong, Interlaminar fracture toughness of composite laminates with CNT-enhanced nonwoven carbon tissue interleave, Composites Science and Technology 73 (2012) 1 – 8, https://doi.org/10.1016/j.compscitech.2012.09.011.

[20] O. Kaynan, Y. Atescan, E. Ozden-Yenigun, H. Cebeci, Mixed mode delamination in carbon nanotube/nanofiber interlayered composites, Composites Part B: Engineering 154 (2018) 186 – 194, https://doi.org/10.1016/j.compositesb.2018.07.032.

[21] X. Du, H. Zhou, W. Sun, H.-Y. Liu, G. Zhou, H. Zhou, Y.-W. Mai, Graphene/epoxy interleaves for delamination toughening and monitoring of crack damage in carbon fibre/epoxy composite laminates, Composites Science and Technology 140 (2017) 123 – 133, https://doi.org/10.1016/j.compscitech.2016.12.028.

[22] X. Xu, Z. Zhou, Y. Hei, B. Zhang, J. Bao, X. Chen, Improving compression-after-impact performance of carbon fiber composites by CNTs/thermoplastic hybrid film interlayer, Composites Science and Technology 95 (2014) 75 – 81, https://doi.org/10.1016/j.compscitech.2014.01.023.

[23] D. Quan, D. Carolan, C. Rouge, N. Murphy, A. Ivankovic, Carbon nanotubes and core–shell rubber nanoparticles modified structural epoxy adhesives, Journal of Materials Science 52 (8) (2017) 4493–4508, https://doi.org/10.1007/s10853-016-0695-9.

[24] D. Quan, D. Carolan, C. Rouge, N. Murphy, A. Ivankovic, Mechanical and fracture properties of epoxy adhesives modified with graphene nanoplatelets and rub-

ber particles, International Journal of Adhesion and Adhesives 81 (2018) 21 – 29, https://doi.org/10.1016/j.ijadhadh.2017.09.003.

[25] K. Dydek, P. Latko-Duralek, A. Boczkowska, M. Salacinski, R. Kozera, Carbon fiber reinforced polymers modified with thermoplastic nonwovens containing multi-walled carbon nanotubes, Composites Science and Technology 173 (2019) 110 – 117, https://doi.org/10.1016/j.compscitech.2019.02.007.

[26] G. W. Beckermann, K. L. Pickering, Mode I and Mode II interlaminar fracture toughness of composite laminates interleaved with electrospun nanofibre veils, Composites Part A: Applied Science and Manufacturing 72 (2015) 11 – 21, https://doi.org/10.1016/j.compositesa.2015.01.028.

[27] B. Beylergil, M. Tanoglu, E. Aktas, Effect of polyamide-6,6 (PA 66) nonwoven veils on the mechanical performance of carbon fiber/epoxy composites, Composite Structures 194 (2018) 21 – 35, https://doi.org/10.1016/j.compstruct.2018.03.097.

[28] B. Beylergil, M. Tanoglu, E. Aktas, Enhancement of interlaminar fracture toughness of carbon fiberepoxy composites using polyamide-6,6 electrospun nanofibers, Journal of Applied Polymer Science 134 (35) (2017) 45244, https://doi.org/10.1002/app.45244.

[29] B. D. Saz-Orozco, D. Ray, A. Kervennic, P. McGrail, W. F. Stanley, Toughening of carbon fibre/polybenzoxazine composites by incorporating polyethersulfone into the interlaminar region, Materials & Design 93 (2016) 297 – 303, https://doi.org/10.1016/j.matdes.2015.12.138.

[30] V. A. Ramirez, P. J. Hogg, W. W. Sampson, The influence of the nonwoven veil architectures on interlaminar fracture toughness of interleaved

composites, Composites Science and Technology 110 (2015) 103 – 110, https://doi.org/10.1016/j.compscitech.2015.01.016.

[31] B. Beylergil, M. Tanoglu, E. Aktas, Mode-I fracture toughness of carbon fiber/epoxy composites interleaved by aramid nonwoven veils, Steel and Composite Structures 31 (2) (2019) 113–123, https://doi.org/10.12989/scs.2019.31.2.113.

[32] B. Beylergil, M. Tanoglu, E. Aktas, Modification of carbon fibre/epoxy composites by polyvinyl alcohol (PVA) based electrospun nanofibres, Advanced Composites Letters 25 (3) (2016) 69–76, https://doi.org/10.1177/096369351602500303.

[33] J. Zhang, T. Yang, T. Lin, C. H. Wang, Phase morphology of nanofibre interlayers: Critical factor for toughening carbon/epoxy composites, Composites Science and Technology 72 (2) (2012) 256 – 262, https://doi.org/10.1016/j.compscitech.2011.11.010.

[34] M. Guo, X. Yi, G. Liu, L. Liu, Simultaneously increasing the electrical conductivity and fracture toughness of carbonfiber composites by using silver nanowires-loaded interleaves, Composites Science and Technology 97 (2014) 27 – 33, https://doi.org/10.1016/j.compscitech.2014.03.020.

[35] D. Quan, C. Mischo, X. Li, G. Scarselli, A. Ivankovic, N. Murphy, Improving the electrical conductivity and fracture toughness of carbon fibre/epoxy composites by interleaving MWCNT-doped thermoplastic veils, Composites Science and Technology 182 (2019) 107775, https://doi.org/10.1016/j.compscitech.2019.107775.

[36] V. Kumar, T. Yokozeki, T. Okada, Y. Hirano, T. Goto, T. Takahashi, T. Ogasawara, Effect of through-thickness electrical conductivity of CFRPs on lightning strike damages, Composites Part A: Applied Science and Manufacturing 114 (2018) 429 – 438, https://doi.org/10.1016/j.compositesa.2018.09.007.

[37] BS ISO 15024:2001, Fibre-reinforced plastic composites Determination of mode I interlaminar fracture toughness, G_{IC} for unidirectionally reinforced materials, International Organization for Standardization (2001).

[38] ISO 15114:2014, Fibre-reinforced plastic composites Determination of mode II fracture resistance for unidirectionally reinforced materials using the calibrated end-loaded split (C-ELS) test and an effective crack length approach, International Organization for Standardization (2014).

[39] F. H. Gojny, M. H. G. Wichmann, U. Kopke, B. Fiedler, K. Schulte, Carbon nanotube-reinforced epoxy-composites: enhanced stiffness and fracture toughness at low nanotube content, Composites Science and Technology 64 (15) (2004) 2363 – 2371, https://doi.org/10.1016/j.compscitech.2004.04.002.

[40] F. Wang, L. T. Drzal, Y. Qin, Z. Huang, Enhancement of fracture toughness, mechanical and thermal properties of rubber/epoxy composites by incorporation of graphene nanoplatelets, Composites Part A: Applied Science and Manufacturing 87 (2016) 10 – 22, https://doi.org/10.1016/j.compositesa.2016.04.009.

[41] S. Chandrasekaran, N. Sato, F. Tlle, R. Mlhaupt, B. Fiedler, K. Schulte, Fracture toughness and failure mechanism of graphene based epoxy composites, Composites Science and Technology 97 (2014) 90 – 99, https://doi.org/10.1016/j.compscitech.2014.03.014.

[42] S. Chandrasekaran, C. Seidel, K. Schulte, Preparation and characterization of graphite nano-platelet (GNP)/epoxy nano-composite: Mechanical, electrical and thermal properties, European Polymer Journal 49 (12) (2013) 3878 – 3888, https://doi.org/10.1016/j.eurpolymj.2013.10.008.

[43] M. R. Ayatollahi, S. Shadlou, M. M. Shokrieh, Fracture toughness of epoxy/multi-walled carbon nanotube nano-composites under bending and shear loading conditions, Materials & Design 32 (4) (2011) 2115 – 2124, https://doi.org/10.1016/j.matdes.2010.11.034.

[44] G. Li, P. Li, C. Zhang, Y. Yu, H. Liu, S. Zhang, X. Jia, X. Yang, Z. Xue, S. Ryu, Inhomogeneous toughening of carbon fiber/epoxy composite using electrospun polysulfone nanofibrous membranes by in situ phase separation, Composites Science and Technology 68 (3) (2008) 987 – 994, https://doi.org/10.1016/j.compscitech.2007.07.010.

[45] L. Daelemans, S. van der Heijden, I. D. Baere, H. Rahier, W. V. Paepegem, K. D. Clerck, Nanofibre bridging as a toughening mechanism in carbon/epoxy composite laminates interleaved with electrospun polyamide nanofibrous veils, Composites Science and Technology 117 (2015) 244 – 256, https://doi.org/10.1016/j.compscitech.2015.06.021.

[46] M. Kuwata, P. J. Hogg, Interlaminar toughness of interleaved CFRP using non-woven veils: Part 1. Mode-I testing, Composites Part A: Applied Science and Manufacturing 42 (10) (2011) 1551 – 1559, https://doi.org/10.1016/j.compositesa.2011.07.016.

[47] M. Kuwata, P. J. Hogg, Interlaminar toughness of interleaved CFRP using non-woven veils: Part 2. Mode-II testing, Composites Part A: Applied Science and Manufacturing 42 (10) (2011) 1560 – 1570, https://doi.org/10.1016/j.compositesa.2011.07.017.

[48] H. Saghafi, A. Zucchelli, R. Palazzetti, G. Minak, The effect of interleaved composite nanofibrous mats on delamination behavior of polymeric composite materials, Composite Structures 109 (2014) 41 – 47, https://doi.org/10.1016/j.compstruct.2013.10.039.

[49] D. W. Wong, L. Lin, P. T. McGrail, T. Peijs, P. J. Hogg, Improved fracture toughness of carbon fibre/epoxy composite laminates using dissolvable thermoplastic fibres,

Composites Part A: Applied Science and Manufacturing 41 (6) (2010) 759 – 767, https://doi.org/10.1016/j.compositesa.2010.02.008.

[50] N. Zheng, Y. Huang, H.-Y. Liu, J. Gao, Y.-W. Mai, Improvement of interlaminar fracture toughness in carbon fiber/epoxy composites with carbon nanotubes/polysulfone interleaves, Composites Science and Technology 140 (2017) 8 – 15, https://doi.org/10.1016/j.compscitech.2016.12.017.

[51] T. Brugo, R. Palazzetti, The effect of thickness of Nylon 6,6 nanofibrous mat on Modes I-II fracture mechanics of UD and woven composite laminates, Composite Structures 154 (2016) 172 – 178, https://doi.org/10.1016/j.compstruct.2016.07.034.

[52] K. Shivakumar, S. Lingaiah, H. Chen, P. Akangah, G. Swaminathan, L. Russell, Polymer nanofabric interleaved composite laminates, AIAA Journal 47 (7) (2009) 1723–1729, https://doi.org/10.2514/1.41791.

[53] S. Alessi, M. Di Filippo, C. Dispenza, M. L. Focarete, C. Gualandi, R. Palazzetti, G. Pitarresi, A. Zucchelli, Effects of Nylon 6,6 nanofibrous mats on thermal properties and delamination behavior of high performance CFRP laminates, Polymer Composites 36 (7) (2015) 1303–1313, https://doi.org/10.1002/pc.23035.

[54] D. Quan, F. Bologna, G. Scarselli, A. Ivankovic, N. Murphy, Interlaminar fracture toughness of aerospace-grade carbon fibre reinforced plastics interleaved with thermoplastic veils, Composites Part A: Applied Science and Manufacturing 128 (2020) 105642, https://doi.org/10.1016/j.compositesa.2019.105642.

Figures

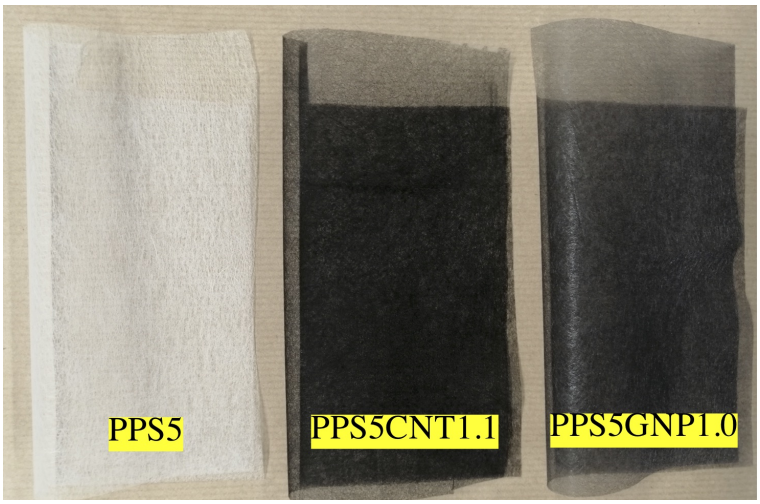

Figure 1: Typical photographs of PPS veils before and after doping with MWCNTs and GNPs.

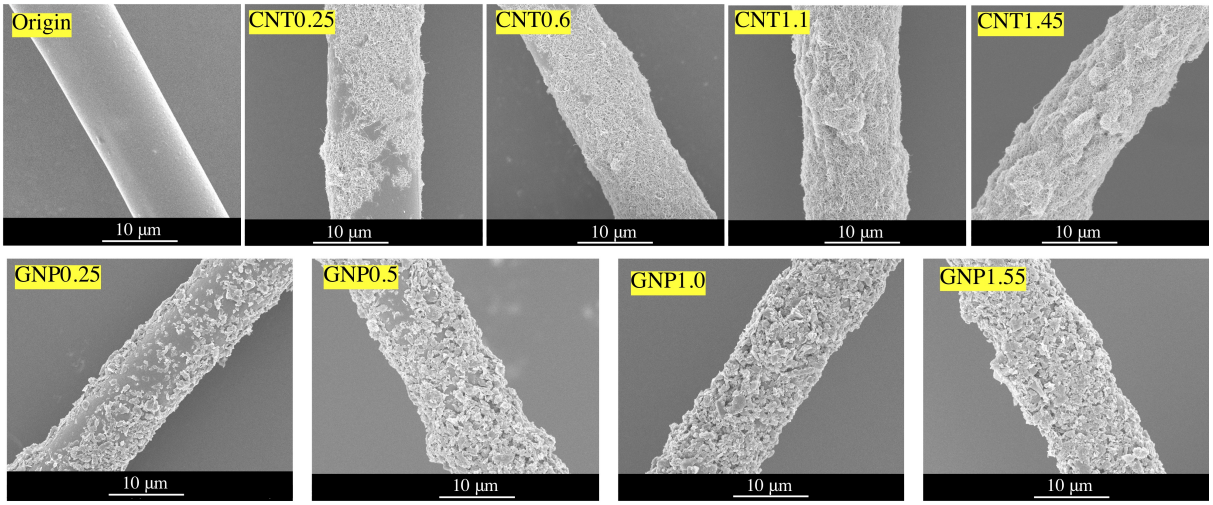

Figure 2: SEM images of individual PPS fibres from the veils before and after doping with MWCNTs and GNPs.

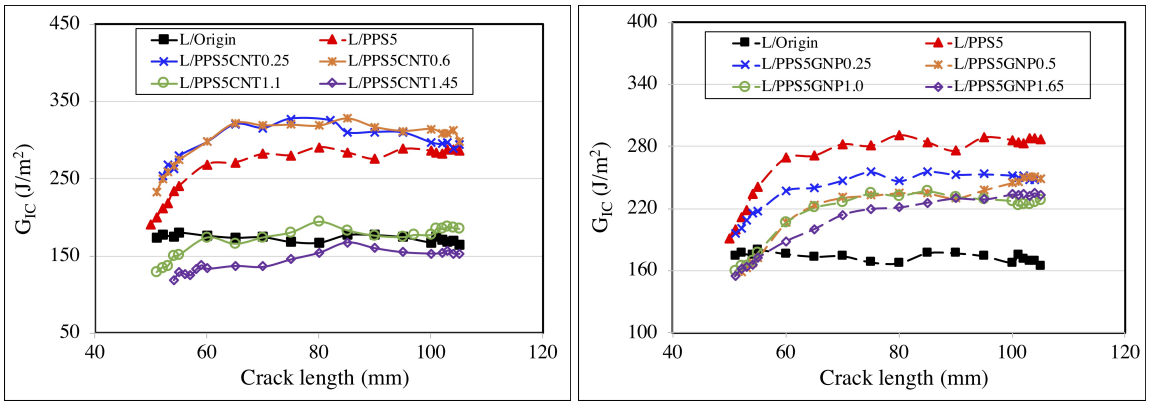

(a) (b)

Figure 3: Typical R-curves from the mode-I DCB tests of the: (a) CFRPs interleaved with MWCNT-doped PPS5 veils; and (b) CFRPs interleaved with GNP-doped PPS5 veils.

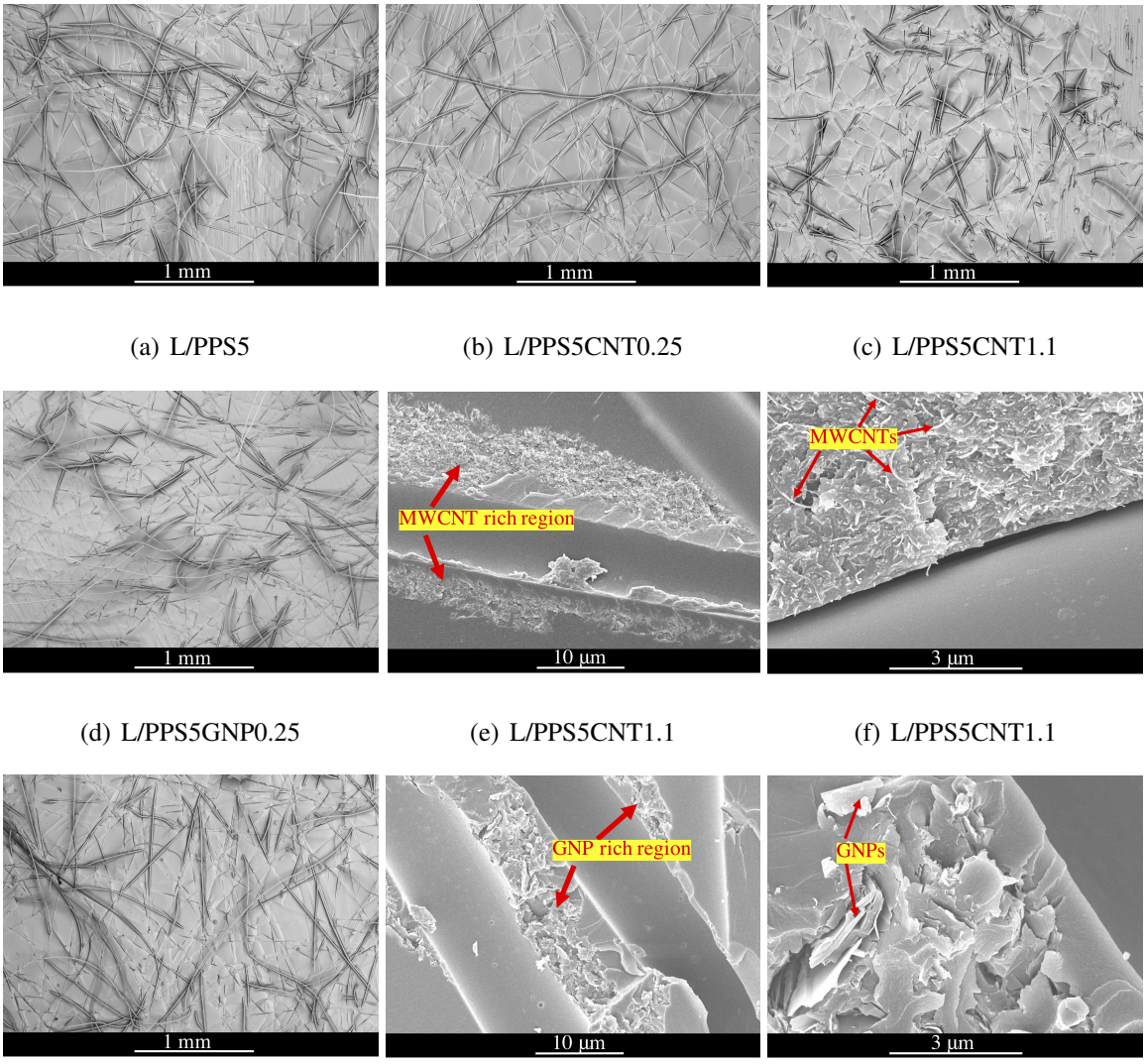

(a) L/PPS5 (b) L/PPS5CNT0.25 (c) L/PPS5CNT1.1

(d) L/PPS5GNP0.25 (e) L/PPS5CNT1.1 (f) L/PPS5CNT1.1

(g) L/PPS5GNP1.0 (h) L/PPS5GNP1.0 (i) L/PPS5GNP1.0

Figure 4: Representative SEM images of the fracture surfaces of the DCB specimens. The magnification is 100 for (a)-(d) and (g), 3 k for (e) and (h) and 15 k for (f) and (i).

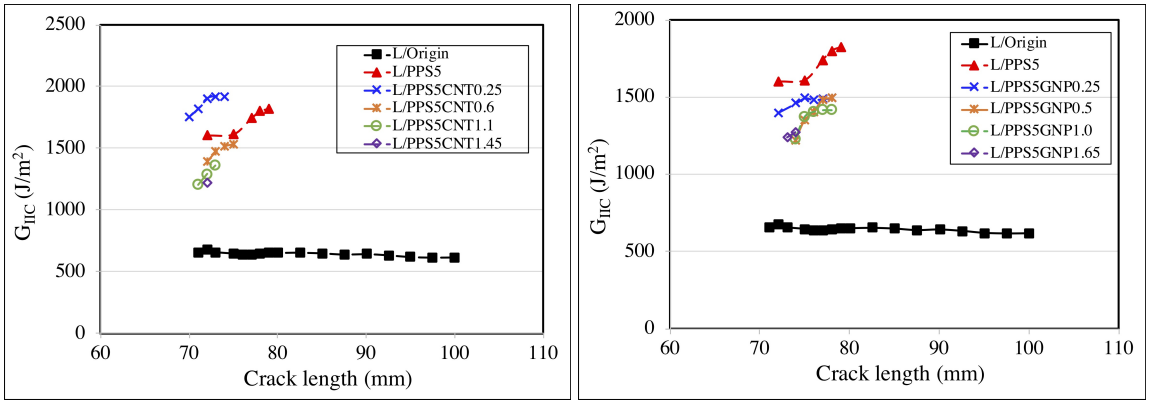

(a) (b)

Figure 5: Typical R-curves from the mode-II ELS tests of the: (a) CFRPs interleaved with MWCNT-doped PPS5 veils; and (b) CFRPs interleaved with GNP-doped PPS5 veils.

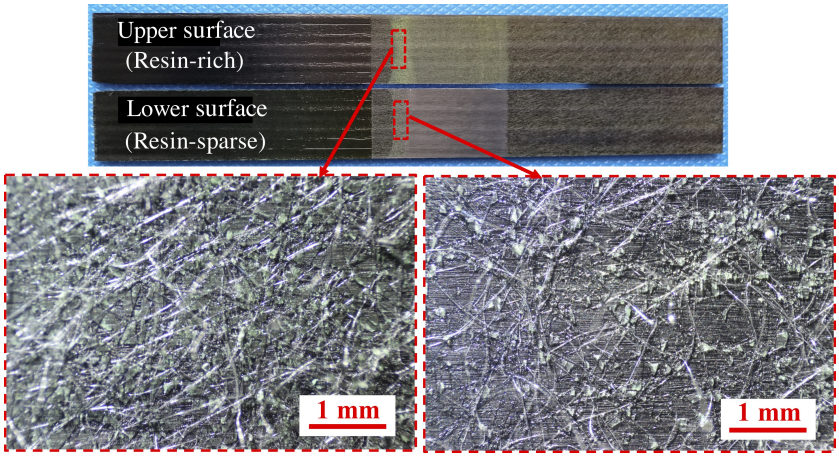

Figure 6: Representative images of the fracture surfaces of an ELS specimen (L/PPS5) as an example for all the interleaved laminates.

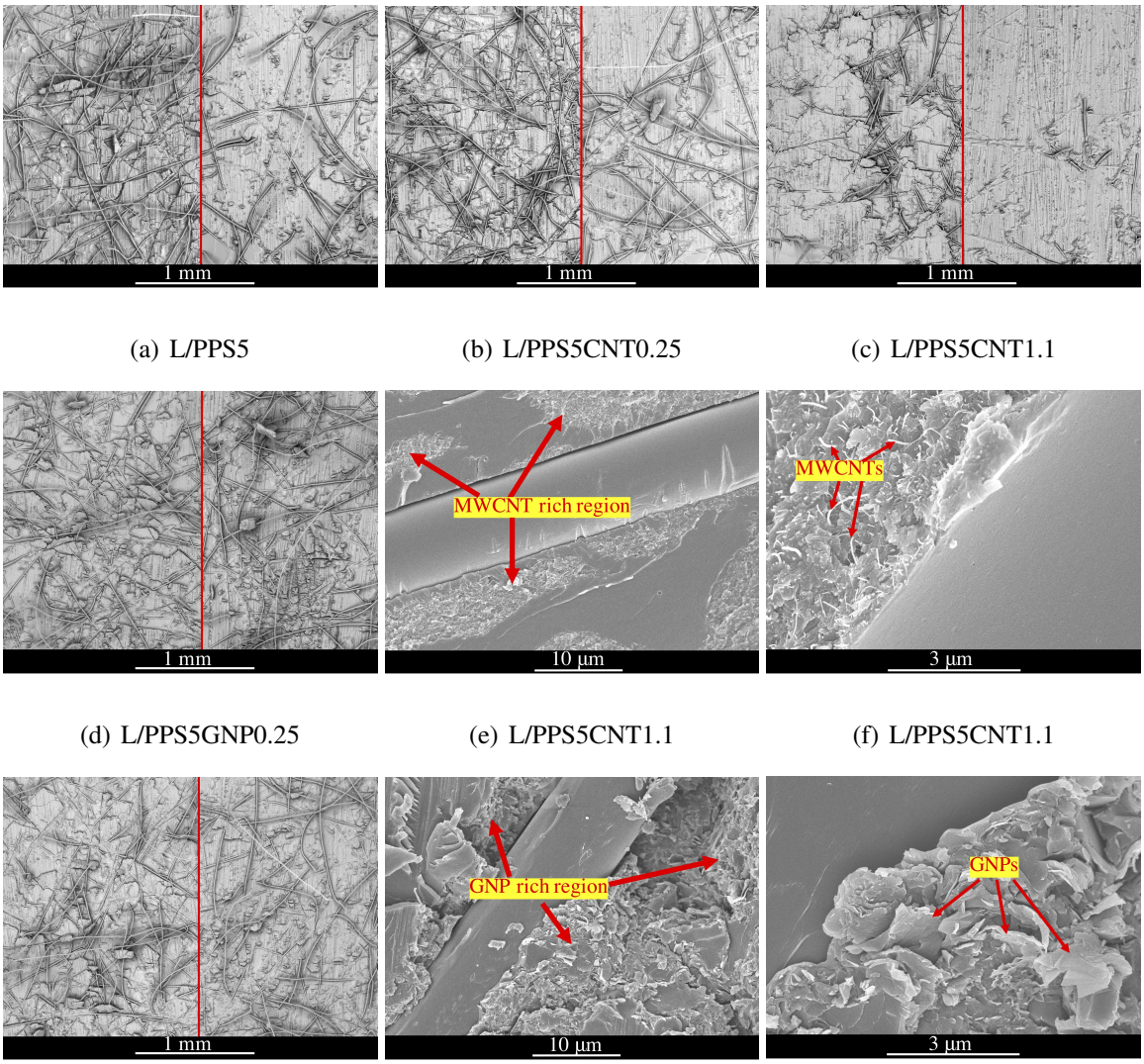

(a) L/PPS5 (b) L/PPS5CNT0.25 (c) L/PPS5CNT1.1

(d) L/PPS5GNP0.25 (e) L/PPS5CNT1.1 (f) L/PPS5CNT1.1

(g) L/PPS5GNP1.0 (h) L/PPS5GNP1.0 (i) L/PPS5GNP1.0

Figure 7: Representative SEM images of the fracture surfaces of the ELS specimens. The images on the left side of the red lines are for the resin-rich side of the fracture surfaces and the images on the right side of the red lines are for the resin-sparse side of the fracture surfaces. The magnification is 100 for (a)-(d) and (g), 3 k for (e) and (h) and 15 k for (f) and (i).

Tables

Table 1: Fracture energy of the CFRPs interleaved with and without PPS veils.

Specimens	G_{IC}^{ini} (J/m^2)	G_{IC}^{prop} (J/m^2)	G_{IIC}^{ini} (J/m^2)	G_{IIC}^{avg} (J/m^2)
L/Origin	181±9	171±8	630±26	627±22
L/PPS5	210±27	264±11	1730±134	1867±136
L/PPS5CNT0.25	247±23	293±13	1892±90	1949±76
L/PPS5CNT0.6	241±17	299±14	1482±59	1497±44
L/PPS5CNT1.1	145±5	181±12	1099±89	1230±48
L/PPS5CNT1.45	126±15	147±6	1271±44	1276±59
L/PPS5GNP0.25	176±19	249±13	1543±99	1627±135
L/PPS5GNP0.5	161±10	228±13	1191±83	1385±61
L/PPS5GNP1.0	155±7	207±18	1121±54	1320±42
L/PPS5GNP1.65	158±16	217±10	1056±127	1151±106

Table 2: Toughening performance of different thermoplastic veils for unidirectional carbon fibre/epoxy composites.

Reference	Polymer (Scale)	Amount of veils	G_{IC} (% increase)	G_{IIC} (% increase)
[44]	PSF (Nano)	1,3,5wt.% of resin	G_{IC}^{avg}:+158,+261,+281%	*
[51]	PA6,6 (Nano)	40μm thick	G_{IC}^{ini}/G_{IC}^{prop}:+56%/+8%	G_{IIC}^{ini}:+61%
[52]	PA6,6 (Nano)	1.6-2.0 g/m^2	G_{IC}^{ini}/G_{IC}^{prop}:+152%/31%	*
[53]	PA6,6 (Nano)	70-100μm thick	G_{IC}^{ini}/G_{IC}^{prop}:+23%/**-22**%	*
[45]	PA6,6 (Nano)	3,18 g/m^2	G_{IC}^{ini}/G_{IC}^{prop}:**-40**,+4%/-41,**-27**%	G_{IIC}^{ini}/G_{IIC}^{prop}:+46,+183%/+42,+188%
	PA6,9 (Nano)	3,18 g/m^2	G_{IC}^{ini}/G_{IC}^{prop}:**-46**,+4%/**-36,-35%**	G_{IIC}^{ini}/G_{IIC}^{prop}:+64,+183%/+67,+211%
[28]	PA6,6 (Nano)	0.525,1.05 g/m^2	G_{IC}^{ini}/G_{IC}^{prop}:+28,+50%/+50,+51%	*
[26]	PA6,6 (Nano)	4.5 g/m^2	G_{IC}^{ini}/G_{IC}^{prop}:+34%/**-6%**	G_{IIC}^{ini}:+69%
	PVB (Nano)	4.3 g/m^2	G_{IC}^{ini}/G_{IC}^{prop}:+16 %/+11%	G_{IIC}^{ini}:**-6%**
	PCL (Nano)	4.2 g/m^2	G_{IC}^{ini}/G_{IC}^{prop}:+4 %/+12%	G_{IIC}^{ini}:+7%
	PES (Nano)	3.6 g/m^2	G_{IC}^{ini}/G_{IC}^{prop}:**-52 %/-52%**	G_{IIC}^{ini}:+20%
	PAI (Nano)	4.1 g/m^2	G_{IC}^{ini}/G_{IC}^{prop}:**-58 %/-68%**	G_{IIC}^{ini}:+56%
[27]	PA6,6 (Micro)	17,50 g/m^2	G_{IC}^{ini}/G_{IC}^{prop}:+84,+349%/+171,+718%	*
[26]	PVB (Micro)	4.5 g/m^2	G_{IC}^{ini}/G_{IC}^{prop}:+13 %/+5%	G_{IIC}^{ini}:**-8%**
[46, 47]	PE (Micro)	23 g/m^2	G_{IC}^{ini}/G_{IC}^{prop}:+65%/+20%	G_{IIC}^{ini}/G_{IIC}^{prop}:+57%/+44%
	PA (Micro)	21 g/m^2	G_{IC}^{ini}/G_{IC}^{prop}:**-55%/-51%**	G_{IIC}^{ini}/G_{IIC}^{prop}:+43%/+92%
[54]	PET (Micro)	8,12,17 g/m^2	G_{IC}^{ini}/G_{IC}^{prop}:+36-127%/+85-173%	*
	PPS (Micro)	5,10,15 g/m^2	G_{IC}^{ini}/G_{IC}^{prop}:+16-74%/+65-216%	*
	PA (Micro)	10,15 g/m^2	G_{IC}^{ini}/G_{IC}^{prop}:+80-86%/+78-85%	*
This study	PPS (Micro)/MWCNTs	5/0.25 g/m^2	G_{IC}^{ini}/G_{IC}^{prop}:+36%/+71%	G_{IIC}^{ini}/G_{IIC}^{avg}:+200%/+211%
	PPS (Micro)/MWCNTs	5/0.6 g/m^2	G_{IC}^{ini}/G_{IC}^{prop}:+33%/+75%	G_{IIC}^{ini}/G_{IIC}^{avg}:+135%/+139%
	PPS (Micro)/GNPs	5/0.25 g/m^2	G_{IC}^{ini}/G_{IC}^{prop}:**-3**%/+46%	G_{IIC}^{ini}/G_{IIC}^{avg}:+145%/+159%
	PPS (Micro)/GNPs	5/0.5 g/m^2	G_{IC}^{ini}/G_{IC}^{prop}:**-11**%/+33%	G_{IIC}^{ini}/G_{IIC}^{avg}:+89%/+121%

* PSF: Polyethersulfone; PVB: Polyvinyl butyral; PCL: Polycaprolactone; PAI: Polyamide-imides; PE: Polyethylene; PET: Polyethylene terephthalate